Self-doping processes between planes and chains in the metal-to-superconductor transition of $YBa_2Cu_3O_{6.9}$

M. Magnuson[1], T. Schmitt[2] V.N. Strocov[2], J. Schlappa[2,3],
A. S. Kalabukhov[4] and L.-C. Duda[5]

[1]*Department of Physics, Chemistry and Biology, IFM, Thin Film Physics Division, Linköping University, SE-58183 Linköping, Sweden*
[2]*Paul Scherrer Institut, Swiss Light Source (SLS), CH-5232 Villigen PSI, Switzerland*
[3]*Institut Methoden und Instrumentierung der Forschung mit Synchrotronstrahlung (G-ISRR), Helmholtz-Zentrum Berlin für Materialien und Energie GmbH, D-12489 Berlin, Germany*
[4]*Quantum Devices Physics Group, Department of Microtechnology and Nanoscience-MC2, Chalmers University of Technology, SE412 96 Gothenburg, Sweden*
[5]*Department of Physics and Astronomy, Division of Molecular and Condensed Matter Physics, Uppsala University, Box 516, S-751 20 Uppsala, Sweden*

Corresponding author: Martin.Magnuson@ifm.liu.se

Supplementary Information

1. Materials and Methods

1.1 Growth of $YBa_2Cu_3O_{6+x}$ films

Thin films of $YBa_2Cu_3O_{6+x}$ (YBCO) were grown by pulsed laser deposition on (100) $SrTiO_3$ 5x5x0.5 mm^3 single crystal substrates using 25 nm thick CeO_2 buffer layers deposited using RF sputtering at a temperature of 780 °C. The layers were deposited with an RF source power of 100 W in a mixed argon-oxygen atmosphere (60% O_2 + 40% Ar) at a partial pressure of 0.1 mbar. The distance between the target and the sample was 30 mm. After CeO_2 deposition, the sample was slowly (10°C/min) cooled down to room temperature under 500 mbar oxygen pressure and was transferred into the PLD chamber without breaking vacuum. During the deposition of YBCO, a substrate was placed directly into the sapphire sample holder and heated by a SiC radiation heater from the back side. The YBCO films were deposited at the temperature of 820 °C. The oxygen pressure during deposition was set to 0.6 mbar, the repetition rate to 10 Hz and the laser energy density at the target 1.25 J/cm^2. The substrate-to-target distance was set to 60 mm. 7500 laser pulses approximately correspond to YBCO thickness of about 350 nm. To obtain optimal doping (x ≈ 0.9), the films were post-annealed in-situ at 550 °C at an oxygen pressure of 750 mbar.

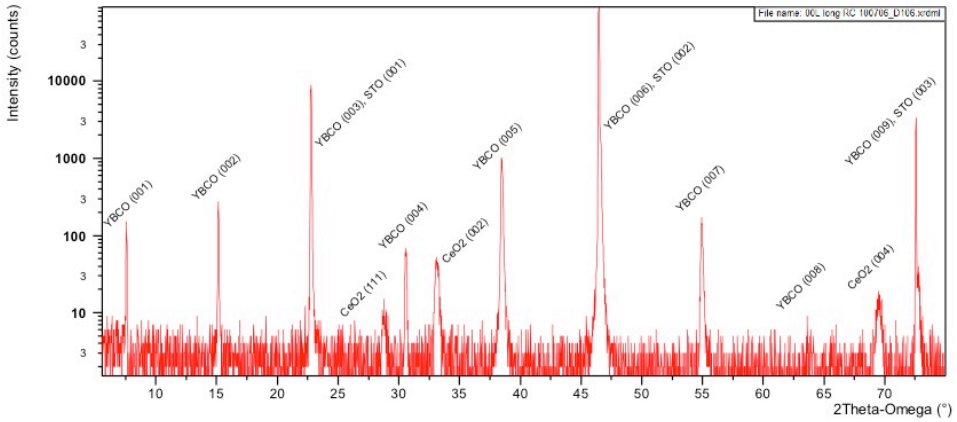

Figure 5: XRD data from optimally doped $YBa_2Cu_3O_{6+x}$ thin films (with x ≈ 0.9).

The critical temperature for superconductivity was determined from magnetic susceptibility measurements by placing the sample between two inductive coils made of copper wire. An external ac current at a frequency of 1 kHz was used to produce a magnetic field in the first coil, while the second coil was used to detect the signal at the same frequency using a lock-in amplifier. The sample was slowly cooled down close to the expected critical temperature. There is a clear decrease of the magnetic susceptibility indicating a transition from a paramagnetic normal state into the diamagnetic superconducting state. Note that the apparent residual susceptibility is due to the geometry of the setup, i.e. the diameter of the induction coils was 10 mm, two times larger than the relatively small sample size of 5x5 mm^2. Although the area ratio was less than 4, a decrease of the signal is also caused by stray fields. The critical temperature can be determined as a temperature corresponding to

the half of the signal at the onset of the superconducting transition. The optimally doped sample ($x \approx 0.9$) has critical temperature of $T_c = 90.5$ K and very sharp transition with $\Delta T_c \approx 1$ K signifying high quality of the sample.

The crystalline quality of the samples was checked by x-ray diffraction (XRD) and was found to be excellent, see Fig. 5 with a typical FWHM of the rocking curve of about 0.1 degrees. Only (00L) peaks of YBCO films have been observed confirming that the films were grown with their c-axis perpendicular to the substrate surface. The XRD data show single-phase c-oriented films with very high crystalline quality. Any inhomogeneity would be observed by a presence of other phases or broadening of the XRD peaks. The doping concentration of each film was determined from unit cell dimensions obtained in X-ray measurements [S1]. The transition temperature of the single-crystalline YBCO was 90.5 K [S2].

1.2 X-ray emission and absorption measurements

The XAS and RIXS measurements were performed at the Advanced Resonant Spectroscopies (ADRESS) beamline [S3] at the Swiss Light Source (SLS), Paul Scherrer Institut, Switzerland, using the Super-Advanced X-ray Emission Spectrometer (SAXES) [S4]. A photon flux of about 10^{13} photons/sec/0.01% bandwidth was focused to a spot size below 5x55 μm vertically and horizontally (VxH). The Cu L_3 edge XAS measurements were made in the bulk-sensitive total fluorescence yield (TFY) mode with an energy resolution of 100 meV. For the RIXS measurements at the Cu L_3 edge (930 eV), the combined energy resolution was 120 meV. To investigate the anisotropy of the electronic structure, linearly polarized x-rays were used at 20^o grazing angle with the electric field vector (**E**) oriented either (nearly) parallel to the *c*-axis (out-of-plane) or parallel to the CuO_2 planes (in-plane) defined by the *a*-axis and the *b*-axis (Fig. 1C).

1.3 Ligand-field multiplet calculations

The Cu $3d \rightarrow 2p$ RIXS spectra of YBCO were calculated as a coherent second-order optical process including interference effects using the Kramers-Heisenberg formula [S5] including interference in the intermediate states. The Slater integrals, describing $3d$ - $3d$ and $3d$ - $2p$ Coulomb and exchange interactions, and spin-orbit constants were obtained by the Hartree-Fock method [S6]. The effect of the configuration-dependent hybridization was taken into account by scaling the Slater integrals to $F_k(3d3d)$ 80%, F_k $(2p3d)$ 80% and G_k $(2p3d)$ 80%. The ground state of the Cu^{2+} ion has $^2D_{5/2}$ character in D_{4h} symmetry. In order to take into account the polarization dependence and exchange interactions, the calculations were also made in the C_{4h} basis set at 0 K. As the Cu electron configurations fluctuate between $3d^{10}$, $3d^9$ and $3d^8$ in the ground state, the wave function contains all three configurations in addition to several charge-transfer configurations that were considered.

The single-impurity Anderson model (SIAM) [S7] with full multiplet effects was applied to describe the system. The crystal field and exchange interactions were taken into account by using a code by Butler [S8] and the charge-transfer effect was implemented with a code by Thole and Ogasawara [S9]. The charge-transfer energy Δ, defined as the energy difference between the centre of gravity between the main line and the different charge-transfer configurations, was chosen to reproduce the experiment (Δ_{gs}=4.1 eV and Δ_{ls}=4.25 eV), the crystal-field splitting in the $3d^9$ D_{4h} local symmetry ($10Dq$=1.5, D_s=0.3, D_t=0.16) with an inter-atomic exchange field (0.21 eV). The three E_{dxy}=-1.49 eV, E_{dxz}=-1.66 eV and E_{dyz}=-1.66 eV orbitals are collectively referred to as t_{2g} and the E_{dx2-y2}=0 and E_{dz2-r2}=-2.01 eV orbitals as e_g. The calculations were made for the same geometry as the experimental one, with the scattering angle between the incoming and outgoing photons fixed to 90^o.

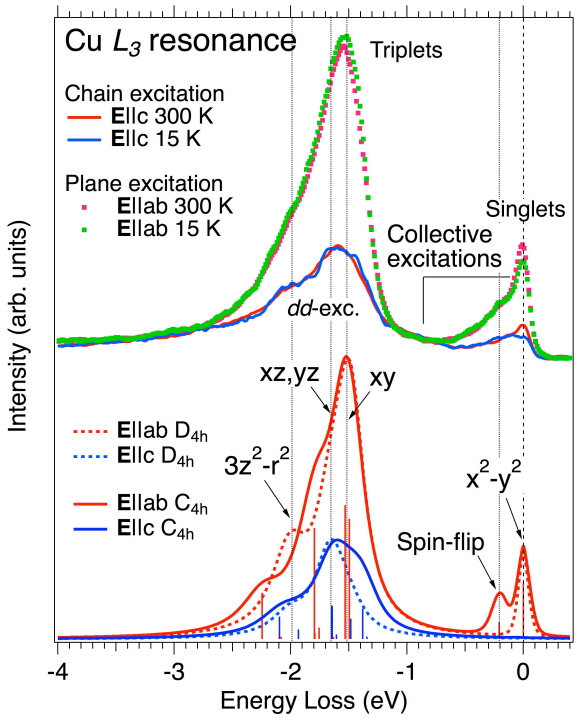

Figure 6: Top: Cu L_3 resonance RIXS spectra excited at 930.7 eV. Bottom: Calculated spectra with $3d^9$ (Cu^{2+}) final states in D_{4h} and C_{4h} symmetry including Cu 3_{dx2-y2} super-exchange energy of 0.21 eV.

The somewhat unusual $3d^8L^{+1}$ state thus corresponds to an extra electron added to the ligand band and could be associated with localized states of Cu(1) close to empty O(1) sites. Note that L^{+1}- and L^{-1}-states are indistinguishable for technical reasons in the ionic calculations. Instead, we make assignments based on physical arguments.

As pointed out in the main text, the four configurations (wherein $3d^9L^{+1}$ and $3d^9L^{-1}$ are calculation-wise indistinguishable) contribute to the total spectrum with different weighting. The significant spectral changes in the RIXS spectra that are observed at the MST can be extracted by taking the difference spectra and compared directly to the spectrum of the pure configurations, reavealing that the observed changes are due to shifting contributions from the $3d^8L^{+1}$ ($3d^9L^{-1}$) configuration for the chain (plane) satellite excitation above and below the MST. As observed in this work, the weight gain of the plane satellite excited RIXS spectra below the MST is due to $3d^9L^{-1}$ and not $3d^9L^{+1}$ as follows from charge conservation arguments and the sign of the difference spectra at the L_3-XAS satellites.

Figure 6 shows a close up of the resonant L_3 spectra in comparison to calculations. Excitation close to the L_3 resonance (929.8 eV and 930.7 eV) yields spectra dominated by *dd*-excitations (of $3d^9$-configuration) that are localized on the highly distorted divalent Cu orbitals *in* (E_{dx2-y2}=0, Ed_{xy}=-1.49 eV) and *perpendicular* to ($E_{d3z2-r2}$=-2.01 eV) the CuO_2-planes. The spin-splitting (superexchange of 0.21 eV) of the highest-lying E_{dx2-y2}=0 orbital is clearly observed and consistent with [12] while the other $3d^9$ orbitals are relegated away from the E_F by the crystal-field effect. The *dd*-orbitals, as well as the spin-excitation peak (paramagnon) observed at -0.21 eV exhibit little spectral shape dependence at the MST [10,14]. Upon cooling, the intensity at 0 eV is lowered as the number of holes is increased and the superconducting gap is formed. As the carriers lower their kinetic energy at the MST, the spectral weight is transferred from the E_F and the elastic peak decreases.

The left panel of Figure 7 shows the temperature dependence of the resonantly excited Cu L_3 spectra with the arrow pointing out the enhancement of the transverse (**E**//**c**) lattice mode at low temperature. The right panel displays a close up of the mid-infrared region fitted

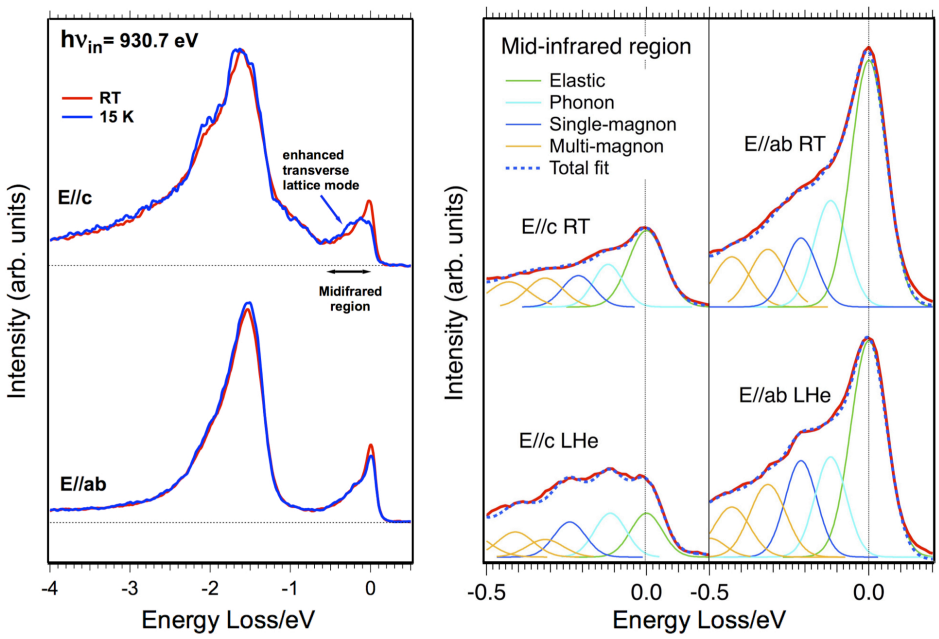

Figure 7: Mid-infrared energy region of the Cu L_3 resonance RIXS spectra excited at 930.7 eV. The spectra are dominated by the elastic peak at 0 eV, a single phonon mode at 116 meV, a single-magnon mode at 230 meV (246 meV out-of-plane) and multi-magnon modes at 320 meV (mainly in-plane) and 390 meV.

with Gaussian functions for **E**//**c** (left) and **E**//**ab** polarizations (right). Adopting the assignments of Ref. 10, the spectra consist of the elastic peak at 0 eV, a single phonon mode at 116 meV, a single-magnon mode at 230 meV (246 meV out-of-plane) and multi-magnon modes at 320 meV (mainly in-plane) and 390 meV. We find that sample cooling leads to a strong increase of the single magnon mode (230 meV for **E**||**ab** and 246 meV for **E**||**c**) and a decrease of a phonon mode (116 meV). Although at this stage, various possibilities must be considered for explaining the nature of these lattice excitations, our observation shows that polarization effects may be as significant as q-dependence effects in RIXS of highly anisotropic systems such as the HTSC cuprates.

References

[S1] P. Benzi, E. Bottizzo, and N. Rizzi; Oxygen determination from cell dimensions in YBCO superconductors, *J. of Cryst. Growth* **269**, 625-629 (2004).

[S2] R. Liang, D. A. Bonn, and W. N. Hardy; Evaluation of CuO_2 plane hole doping in $YBa_2Cu_3O_{6+x}$ single crystals, *Phys. Rev. B* **73**, 180505R (2006).

[S3] G. Ghiringhelli *et al.*; SAXES, a high resolution spectrometer for resonant x-ray emission in the 400-1600eV energy range, *Rev. Sci. Instrum.* **77**, 113108 (2006).

[S4] V.N. Strocov, *et al.*; High-resolution soft X-ray beamline ADRESS at the Swiss Light Source for resonant inelastic X-ray scattering and angle-resolved photoelectron spectroscopies, *J. Synchr. Rad.* **17**, 631 (2010).

[S5] H. A. Kramers and W. Heisenberg; Über die streuung von strahlung durch atome, *Z. Phys.* **31**, 681 (1925).

[S6] R. D. Cowan; *The theory of atomic structure and spectra* (Berkeley, CA: University of California Press) (1981).

[S7] P. W. Anderson; Localized magnetic states in metals; *Phys. Rev. B* **41**, 124 (1961).

[S8] P. H. Butler, *Point group symmetry applications: methods and tables* (New York: Plenum) (1981).

[S9] F. de Groot and A. Kotani; *Core level spectroscopy of Solids:* (CRC Press) (2008).

[S10] J. Schlappa *et al.*; Spin-orbital separation in the quasi-one-dimensional Mott insulator Sr_2CuO_3, *Nature* **485**, 82 (2012).